RESEARCH ARTICLE

Modeling of contact temperatures and their influence on the tribological performance of PEEK and PTFE in a dual-pin-on-disk tribometer

Zhibin LIN[1], **Ting QU**[1], **Ke ZHANG**[2], **Qingbin ZHANG**[1], **Shengdao WANG**[2], **Guibin WANG**[2], **Bingzhao GAO**[3,*], **Guowei FAN**[4,*]

[1] *State Key Laboratory of Automotive Simulation and Control, Jilin University, Changchun 130025, China*

[2] *Key Laboratory of High Performance Plastics, Ministry of Education, Jilin University, Changchun 130012, China*

[3] *Clean Energy Automotive Engineering Center, Tongji University, Shanghai 201804, China*

[4] *College of Instrumentation and Electrical Engineering, Jilin University, Changchun 130061, China*

© The author(s) 2022.

Abstract: The direct blending of polyether ether ketone (PEEK) with a solid lubricant such as polytetrafluoroethylene (PTFE) improves its tribological performance, but compromises its outstanding mechanical properties and processability. While these negative effects might be circumvented via the hybrid wear method, the influence of the contact temperature between multiple sliding components acting together is not fully understood. Herein, an analytical temperature model considering the influence of both micro- and macro-thermal behavior is extended to predict the contact temperature of a dual-pin-on-disk hybrid wear system. The interactions between several heat sources are investigated and experimentally verified. The analytical results show that the nominal temperature rise of the shared wear track is determined by the combined effect of the heat generated by both pin components, while the rise in flash temperature at the region in contact with each pin component is dependent upon its individual characteristics and working conditions. Hence, while different temperature peaks can coexist in the shared wear track, the maximum value dominates the performance of the system. For the experimentally investigated PEEK–PTFE–steel hybrid wear system, the formation of tribofilms is blocked, and the hybrid wear system fails, when the peak temperature exceeds the glass transition temperature of both pins due to an increase in applied load.

Keywords: contact temperature; frictional heating; dual-pin-on-disk; hybrid wear

1 Introduction

Due to excellent properties such as self-lubrication, corrosion resistance, and insulation, the polymer composites are gradually replacing metals as anti-wear components in the automotive, aerospace, marine, and other industrial fields [1–3]. However, the tribological performance of the unfilled polymer material tends to be poor, with a large friction coefficient [4] or wear rate [5]. While this is generally improved by blending with various types of filler, such as solid lubricants

(e.g., polytetrafluoroethylene (PTFE) or graphite) [6, 7], nanoparticles (e.g., Bi_2O_3, SiO_2, or CuO) [8], and micron-sized particles (e.g., bronze or Al_2O_3) [9], such fillers may compromise the excellent mechanical properties of the matrix polymer [10]. In addition, this method may increase the viscosity of the polymer melt, thereby weakening the processability via injection molding [11, 12].

To avoid the negative effects of direct blending upon the mechanical properties and processability, a method of combining various types of polymer

Nomenclature

$A_{\mathrm{r}i}$	Real contact area in the contact region between Pin (i) and Disk (3) (m^2)	$Q_{i3\mathrm{pin}}$	Heat flow entering Pin (i) within contact region of Pin (i) and Disk (3) (W)
d	Diameter of test ring (m)	r	Radius of specimen pin (m)
D	Diameter of equivalent disk of the test ring assembly (m)	$r_{\mathrm{a}i}$	Load independent radius of a contacting asperity (m)
F_i	Applied load on Pin (i) (N)	r_{ji}	Radius of each asperity in the contact region between Pin (i) and Disk (3) (m)
F_{s}	Seizure load (N)		
h_{c}	Average convective heat transfer coefficient of rotating test ring assembly (W/(m^2·°C))	R	Distance between the axis of the pin and ring (m)
		S	Area of the expose surface of the test ring assembly (m^2)
H_i	Hardness of Pin (i) (MPa)		
K_i	Thermal conductivity of Component (i) (W/(m·°C))	T_{amb}	Ambient temperature (°C)
		T_{c}	Peak contact temperature (°C)
l	Length of specimen pin (m)	$T_{\mathrm{c}i}$	Peak contact temperature of the sliding surface of Pin (i) (°C)
L	Sliding distance (m)		
N_i	Number of contacting asperities on the contact region between Pin (i) and Disk (3) (m)	$T_{\mathrm{c}3-i}$	Peak contact temperature of steel ring in region contact with Pin (i) (°C)
Pe	Peclet number	ΔT_{f}	Transient flash temperature rise (°C)
$q_{i3\mathrm{pin}-\mathrm{n}}$	Nominal heat fluxes entering Pin (i) within contact region of Pin (i) and Disk (3) (W/m^2)	$\Delta T_{\mathrm{f}i}$	Transient flash temperature rise of pin (i) (°C)
		$\Delta T_{\mathrm{f}3-i}$	Transient flash temperature rise of steel ring in region contact with Pin (i) (°C)
$q_{i3\mathrm{pin}}$	Heat fluxes entering the real contact area of Pin (i) within the contact region of Pin (i) and Disk (3) (W/m^2)	T_{g}	Glass transition temperature (°C)
		T_{mea}	Measured temperature of steel ring surface (°C)
$q_{i3\mathrm{disk}}$	Heat fluxes entering the real contact area of the disk within contact region of Pin (i) and Disk (3) (W/m^2)	ΔT_{n}	Nominal temperature rise (°C)
		$\Delta T_{\mathrm{n}i}$	Nominal temperature rise of Component (i) (°C)
		v	Sliding velocity of specimen pin on the ring (m/s)
		w	Angular velocity of test ring rotation (rad/s)
Q_{i3}	Heat flow generated within contact region between Pin (i) and Disk (3) (W)	μ_i	Friction coefficient of Pin (i)
		κ_3	Thermal diffusivity of Steel ring (3) (m^2/s)
$Q_{i3\mathrm{disk}}$	Heat flow entering Disk (3) within contact region of Pin (i) and Disk (3) (W)	α_i	Partitioning fraction of heat entering Pin (i) within contact region of Pin (i) and Disk (3)

composite has attracted attention for improving the tribological performance [13–16]. In the hybrid wear method, one component of the conventional dual-material friction pair is separated into several independent components with individual compositions and functions. The hybrid wear system allows the composition of each component of the friction pair to be independently designed in order to selectively retain its good performance according to the specific requirements, thereby increasing the potential application scope of the polymer composite wear

system. In addition, this approach offers greater freedom and broadens the range of lubricant material choices in the design of wear systems. For example, Balic and Blanchet [17] improved the friction and wear performance of Al sliding against a Cu countersurface by adopting an independent PTFE component. The friction coefficient and wear rate of the aluminum were shown to decrease from 0.6 and 6×10^{-3} mm^3/(N·m) to 0.3 and 1×10^{-3} mm^3/(N·m), respectively.

Based on the above discussion, hybrid wear

systems are clearly worthy of further investigation. However, the conventional test methods such as single-pin-on-disk and ring-on-block friction pairs do not meet the requirements for exploring the interactions between multiple components. For instance, Lin et al. [15, 16] recently explored the tribological performance of pure polyether ether ketone (PEEK) in the presence of an independent PTFE/bronze composite using a dual-pin-on-disk apparatus. Their results demonstrated that the hybrid wear method significantly increased the wear resistance of pure PEEK from 10^{-5} mm^3/(N·m) to a level comparable to those of the blending method ($< 10^{-7}$ mm^3/(N·m)) without compromising its excellent original properties. However, the load-carrying capacity that directly decides the applicability of the hybrid wear system remained unclear.

The load-bearing capacity of the polymer composite wear system is often limited by the contact temperature conditions [18]. The melting point of polymer materials is much lower than that of metals. Therefore, both the mechanical and tribological properties of polymer composites are sensitive to the operating temperature. High contact temperatures induced by a high-temperature environment or large pressure–velocity (PV) operating conditions often lead to early failure of the polymer material due to severe wear [19, 20]. Additionally, polymer materials have very low thermal conductivities compared to metals [21]. This makes them very poor conductors and dissipaters of the heat generated at the contact region, thereby resulting in a high contact temperature. Therefore, an investigation of the load-carrying capacity of the polymer-composite-containing hybrid wear system should be performed in combination with an investigation of the contact temperature.

It is difficult to measure the contact temperature at the actual micro-scale contact region (governed by the surface roughness Ra) under sliding wear conditions due to the presence of transient flash temperatures [22]. Therefore, methods of estimation such as finite element numerical models [23, 24] and analytical methods [25, 26] have been developed to predict the temperature field at the micro-contact region. The latter are more suitable for making preliminary estimates because they do not require the process of modeling needed for the numerical method. Therefore,

their application is not constrained by the specific sample size. However, while the existing analytical method has provided good estimates for the contact temperature of a single-pin-on-disk configuration [25, 27, 28], this method cannot be applied directly to the dual-pin-on-disk configuration due to the presence of multiple macro-scale heat sources in the same wear track. Hence, the potential interactions between these macro-scale heat sources should be addressed properly.

In the present study, an analytical method is developed to predict the contact temperature of a dual-pin-on-disk configuration, and the corresponding experiments are designed and performed. The effects of the applied load and the contact temperature upon the tribological performance of the hybrid wear system are investigated by combining the predicted contact temperature with the experimental results. In addition, observations of the tribofilms and their worn surfaces are used to investigate the wear mechanism and to verify the accuracy of the analytical thermal model.

2 Analytical thermal model of the dual-pin-on-disk setup

2.1 Dual-pin-on-disk setup

As shown schematically in Fig. 1, the dual-pin-on-disk configuration explored herein consists of the two stationary polymer pins labelled Pins (1) and (2) and a rotating Steel ring (3). Each specimen pin is a cylinder with radius r, length l, and flat end faces. One end of each pin is fixed in the pin holder, while the other end is pressed onto the surfaces of the test ring with axial loads of F_1 and F_2. The test ring with a diameter of d is mounted on a pivot-like disk holder, such that both test ring and holder rotate synchronously at an angular speed of w. The two specimen pins are arranged symmetrically with respect to the axis of the test ring, so that they are constrained to slide in the same wear track on the steel ring surface during tests. The distance between the axis of the fixed pin and the rotation ring is R.

During the sliding process, the actual contact area is often much smaller than the nominal contact
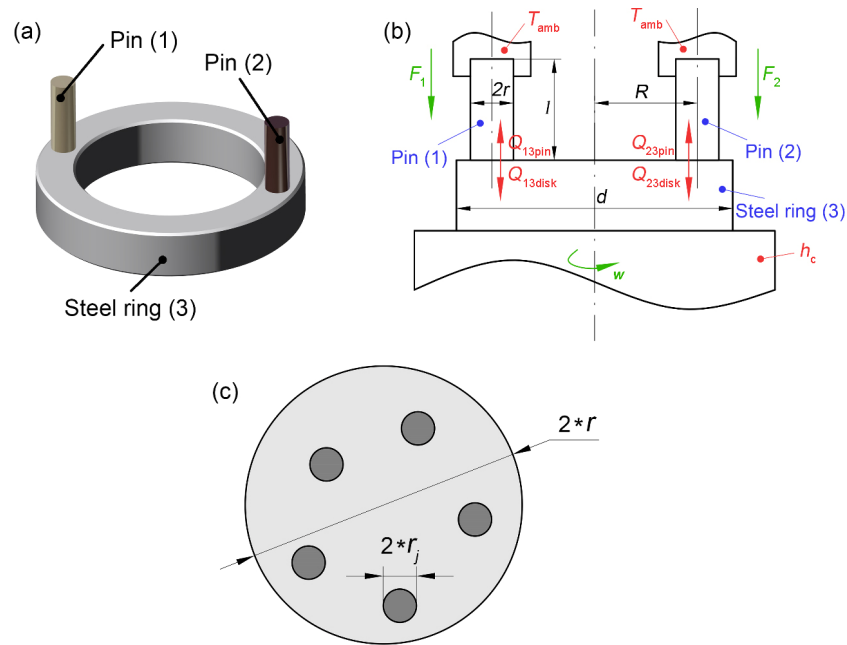
Fig. 1 Dual-pin-on-disk configuration: (a) computer-generated three-dimensional (3D) image, (b) two-dimensional (2D) schematic diagram, and (c) plan view of the contact surface of the pin specimen, in which the dark regions represent the individual actual contact areas and the light region represents the nominal contact surface.

area due to the presence of Ra [29, 30, 31]. Moreover, the actual contact area of the sliding surface is determined not only by Ra, but also by the applied load and the elastic and plastic properties of the material. The contact surface undergoing both plastic and elastic deformation is often composed of multiple micro-contact regions or junctions with generally complex shapes. These factors all create difficulties for the accurate estimation of the actual contact conditions. Hence, researchers have developed a number of methods for estimating the actual contact area on the basis of idealized assumptions. For example, the contact models of Greenwood and Williamson [32] and McCool [33], in which the surface asperity heights are assumed to follow a Gaussian distribution and the contact asperities are hemispheres, have been used to estimate both the actual contact area and the number of contacts from the measured topographical data. Numerical methods have also been used to predict the sliding contact state [34]. Meanwhile, Ashby and Tabor [35, 36] introduced an empirical formula relating the contact area to the property (i.e., the hardness H) of the plastically-deformed softer material. In addition, some novel measurement devices have been developed to directly

measure the actual contact area for characterization of the sliding contact state [37].

Given the large difference in H between the polymer pin and the steel ring in the present study, the contact model assumes that the deformations occurring in the contact regions are all plastic deformation at the surface of the softer polymer pin (Fig. 1(c)). Since the flat end surface of the pin is in plane contact with the topologically isotropic disk, it is assumed that the actual contact area consists of several uniformly-distributed circular contact asperities of the same size, and that the temperature fields for the individual contacts do not interact. The actual contact areas of Pins (1) and (2) are then denoted as A_{r1} and A_{r2}, and are given by Eqs. (1) and (2), respectively:

$$A_{r1} = N_1 \pi r_{j1}^2 \tag{1}$$

$$A_{r2} = N_2 \pi r_{j2}^2 \tag{2}$$

where r_{j1} and r_{j2} are the radii of each asperity in the regions of contact between Pin (1) and Steel ring (3), and between Pin (2) and Steel ring (3), respectively, and N_1 and N_2 are the numbers of contacting asperities formed in the contact regions.

Most researchers agree that approximately all of the

frictional energy (> 95%) dissipating in the contact region is transformed into heat [38, 39]. Therefore, it is assumed that all of the frictional energy is dissipated as heat at the sliding surfaces, and the heat is conducted uniformly through the two contacting bodies as a heat flow within the actual contact area. During sliding, the total heat flow generated within the contact area between Pin (1) and Disk (3), denoted as Q_{13}, and between Pin (2) and Disk (3), denoted as Q_{23}, is given by Eqs. (3) and (4):

$$Q_{13} = \mu_1 F_1 v = \mu_1 F_1 wR \tag{3}$$

$$Q_{23} = \mu_2 F_2 v = \mu_2 F_2 wR \tag{4}$$

where μ_1 and μ_2 are the measured friction coefficients of Pins (1) and (2) under axial loads of F_1 and F_2, respectively; v is the sliding velocity; w is the rotational velocity; and R is the distance between the axis of the fixed pin and the rotation ring (Fig. 1(b)). The parameters Q_{13} and Q_{23} can be further divided into the heat flow entering the pin body (Q_{pin}) and the heat flow entering the disk body (Q_{disk}), as given by Eqs. (5) and (6):

$$Q_{13} = Q_{13\text{pin}} + Q_{13\text{disk}} \tag{5}$$

$$Q_{23} = Q_{23\text{pin}} + Q_{23\text{disk}} \tag{6}$$

2.2 Development of the theoretical analysis method

2.2.1 Contact temperature model

The highest temperature under typical dry sliding conditions occurs at the actual micro-contact region between the two sliding surfaces. Based on the previous work [25, 40], the peak contact temperature of a sliding surface T_c can be determined using Eq. (7):

$$T_c = T_{\text{amb}} + \Delta T_n + \Delta T_f \tag{7}$$

where T_{amb} is the ambient temperature, ΔT_n is the nominal temperature rise (or called bulk surface temperature rise) that occurs a few tens of microns below the actual contact surface, and ΔT_f is the transient flash temperature rise at the points of actual contact.

ΔT_n is caused by the macro heat accumulation due to the repetitive operation of the heat source over the sliding surfaces, and it is influenced by the large-scale heat flow. However, the flash temperature rise ΔT_f,

at the micro-contact point of the actual contact area is determined by the micro-scale heat flow properties. It has been proven that ΔT_f is not affected by large-scale thermal behavior, such as thermal convection and radiation [41, 42]. A simple method can be used to distinguish between these two temperature contributions. When a micro plateau region of the sliding surface comes into contact, its instantaneous temperature rises sharply due to the generation of frictional heat; this transient temperature rise is defined as ΔT_f. ΔT_f disappears quickly when the micro-region is disengaged as the sliding process continues. The remaining temperature rise above T_{amb} at this region is ΔT_n [43].

ΔT_n plays an important role in improving the accuracy of temperature prediction models. Because ΔT_f is often higher than ΔT_n, several studies have treated the predicted flash temperature rise as equal to the maximum surface contact temperature [44, 45]. However, it should be noted that ΔT_f is always calculated on the assumptions that the counter surface is semi-infinite and that all the heat generated is rapidly dissipated by thermal conduction without accumulation. In practice, however, the finite size of the sliding bodies leads to increased temperature of the sliding components due to the continuous accumulation of heat, thereby leading to inaccuracy in the method that considers only ΔT_f. This was verified by Rowe et al. [37], who demonstrated that the calculated flash temperature agreed well with the measured peak contact temperature during the initial stages of the experiment or under the application of forced cooling, but the measured T_c became significantly higher than the estimated flash temperature due to heat accumulation as the experiment progressed. Meanwhile, Kennedy et al. [25, 46] significantly improved the accuracy of the temperature prediction model by considering the effects of ΔT_n due to the large-scale thermal behavior (i.e., thermal convection and conduction). Hence, the present study considers the effects of ΔT_n. The expressions presented herein are relevant for quasi-steady-state conditions.

2.2.2 Contact temperature of the stationary pin

The stationary pin is assumed to be cooled only by the thermal conduction along its axial surface that is directly connected to the steel pin-holder. However,

the natural convection and radiation losses along its lateral surface are neglected because they are too small under this condition. Considering the comparatively large heat capacity of the pin-holder, which is directly connected to the device substrate, it is also assumes that the heat flow entering the pin holder does not cause any temperature rise. Therefore, as a boundary condition for solving the ΔT_n of the pin surface, the surface temperature at the end of the pin that is connected to the pin-holder is held at T_{amb}.

Based on the 2D axisymmetric heat analytical model of Ashby et al. [35], which considers the heat conduction behavior, the ΔT_n at the contact surface of the specimen pin can be expressed by Eqs. (8) and (9):

$$\Delta T_{n1} = q_{13pin-n} \frac{l}{K_1} = \frac{Q_{13pin}}{\pi r^2} \frac{l}{K_1} \qquad (8)$$

$$\Delta T_{n2} = q_{23pin-n} \frac{l}{K_2} = \frac{Q_{23pin}}{\pi r^2} \frac{l}{K_2} \qquad (9)$$

where $q_{13pin-n}$ and $q_{23pin-n}$ are the nominal heat fluxes entering the bodies of Pins (1) and (2), respectively, and K_1 and K_2 are the thermal conductivities of the pin materials, and are assumed to be uniform and constant.

In the case of uniform heat flux over a circular region, Jaeger [47] indicated that the ΔT_f of the pin surface can be determined by Eqs. (10) and (11):

$$\Delta T_{f1} = q_{13pin} \frac{r_{j1}}{K_1} = \frac{Q_{13pin} r_{j1}}{A_{r1} K_1} \qquad (10)$$

$$\Delta T_{f2} = q_{23pin} \frac{r_{j2}}{K_2} = \frac{Q_{23pin} r_{j2}}{A_{r2} K_2} \qquad (11)$$

where q_{13pin} and q_{23pin} are the average heat fluxes flowing into the actual contact area of the pin surface.

The resulting T_c on the two pin surfaces can then be determined by inserting Eqs. (8) and (10) or Eqs. (9) and (11) into Eq. (7) to obtain Eqs. (12) and (13), respectively:

$$T_{c1} = T_{amb} + \frac{Q_{13pin}}{\pi r^2} \frac{l}{K_1} + \frac{Q_{13pin} r_{j1}}{A_{r1} K_1} \qquad (12)$$

$$T_{c2} = T_{amb} + \frac{Q_{23pin}}{\pi r^2} \frac{l}{K_2} + \frac{Q_{23pin} r_{j2}}{A_{r2} K_2} \qquad (13)$$

2.2.3 Contact temperature of the rotating disk

The rise in nominal contact temperature of the rotating disk in the steady-state can be determined by the thermal balance between the heat flow entering the contact surface and the heat removed, which has been proven to have a high prediction accuracy [48, 49]. Since the contact surface between the steel ring and the disk-holder is smooth and both components are relatively stationary during the test, the heat transfer efficiency between them is very high. However, the heat transfer between the rotating disk-holder and the device is more-or-less blocked by the large thermal resistance between the inner and outer rings of the connecting ball bearings. Therefore, it is assumed that the thermal contact between the rotating test ring and the disk-holder is perfect, with zero thermal resistance, while the heat flow between the rotating assembly and the device substrate is completely blocked. Hence, the synchronously rotating test ring and disk holder are considered as a whole part called the test ring assembly. Unlike the stationary pin, the test ring assembly suffers intense forced convection on its exposed surface due to the high-speed rotation, thereby becoming the main source of heat loss. Additionally, due to the good thermal conductivity of steel, it is assumed that the temperature of the exposed surface of the rotating assembly is uniform and equal to the nominal temperature of the steel ring. Therefore, the thermal balance between the heat flow entering the test ring assembly and that removed to the air is given by Eq. (14):

$$Q_{13disk} + Q_{23disk} = h_c S \Delta T_{n3} \qquad (14)$$

where h_c is the average convective heat transfer coefficient between the rotating surface and the air, which can be determined using the empirical equations given by Kreith and Manglik [50] based on the working conditions; S is the total area of the exposed surface of the test ring assembly; and ΔT_{n3} is the nominal temperature rise of the test ring. Hence, we obtain Eq. (15):

$$\Delta T_{n3} = \frac{Q_{13disk} + Q_{23disk}}{h_c S} \qquad (15)$$

The moving circular heat source temperature model

can be used to estimate the ΔT_f of the rotating steel ring [51, 52]. The ΔT_f of the steel ring surface in contact with Pin (1), i.e., ΔT_{f3-1}, and Pin (2), i.e., ΔT_{f3-2}, can be determined by Eqs. (16) and (17):

$$\Delta T_{f3-1} = \frac{2q_{13\text{disk}}r_{j1}}{K_3\sqrt{\pi(1.273+Pe_1)}} = \frac{2Q_{13\text{disk}}r_{j1}}{A_{r1}K_3\sqrt{\pi(1.273+Pe_1)}} \tag{16}$$

$$\Delta T_{f3-2} = \frac{2q_{23\text{disk}}r_{j2}}{K_3\sqrt{\pi(1.273+Pe_2)}} = \frac{2Q_{23\text{disk}}r_{j2}}{A_{r2}K_3\sqrt{\pi(1.273+Pe_2)}} \tag{17}$$

where $q_{13\text{disk}}$ and $q_{23\text{disk}}$ are the average heat fluxes flowing into the steel ring within the real contact region connected with Pins (1) and (2), respectively; and K_3 is the thermal conductivity of steel ring. Pe is the non-dimensional Peclet number defined by $Pe_i = \frac{vr_{ji}}{2\kappa_3}$, where r_{ji} is the radius of the real contact region; v is the sliding velocity; and κ_3 is the thermal diffusivity of the steel ring.

The resulting peak temperatures of the steel ring surface in the regions in contact with Pins (1) and (2) can then be obtained by inserting Eqs. (15) and (16) or (15) and (17) into Eq. (7) to give Eqs. (18) and (19), respectively:

$$T_{c3-1} = T_{\text{amb}} + \frac{Q_{13\text{disk}}+Q_{23\text{disk}}}{h_c S} + \frac{2Q_{13\text{disk}}r_{j1}}{A_{r1}K_3\sqrt{\pi(1.273+Pe_1)}} \tag{18}$$

$$T_{c3-2} = T_{\text{amb}} + \frac{Q_{13\text{disk}}+Q_{23\text{disk}}}{h_c S} + \frac{2Q_{23\text{disk}}r_{j2}}{A_{r2}K_3\sqrt{\pi(1.273+Pe_2)}} \tag{19}$$

Thus, the derivation process indicates that the nominal contact temperature rise of the test ring in the double-pin-on-disk configuration is determined by the combined influence of the heat generated by the two specimen pins because they work in the same wear track and accumulate heat together. However, the ΔT_f of the test ring at the region in contact with the two specimen pins is strongly dependent upon the contact conditions of each specimen pin. This situation allows the test ring to have two different temperature

peaks (T_{c3-1} and T_{c3-2}) in the same wear track under hybrid wear conditions. However, the tribological performance of the system often depends upon the overall maximum value.

2.2.4 Partitioning of frictional heat

The fractions of the frictional heat entering the stationary pin are defined as α_1 and α_2 in the region of Steel ring (3) surface in contact with Pins (1) and (2), respectively. Using Eqs. (3) and (4), we get Eqs. (20–23):

$$Q_{13\text{pin}} = \alpha_1 Q_{13} \tag{20}$$

$$Q_{13\text{disk}} = (1-\alpha_1)Q_{13} \tag{21}$$

$$Q_{23\text{pin}} = \alpha_2 Q_{23} \tag{22}$$

$$Q_{23\text{disk}} = (1-\alpha_2)Q_{23} \tag{23}$$

Blok [53] postulated that the temperatures of the two contact surfaces must be equal within the actual contact areas, but need not be equal elsewhere within the nominal contact area. This method provides a good estimate [46]. Therefore, the heat partition fraction can be calculated by equating the maximum surface temperatures of the contact surfaces, as in Eqs. (24) and (25):

$$T_{c1} = T_{c3-1} \tag{24}$$

$$T_{c2} = T_{c3-2} \tag{25}$$

Using Eqs. (12), (13), (18), and (19) in Eqs. (24) and (25), we get Eqs. (26) and (27):

$$\frac{\alpha_1 Q_{13}}{\pi r^2}\frac{l}{K_1} + \frac{\alpha_1 Q_{13}r_{j1}}{A_{r1}K_1} = \frac{(1-\alpha_1)Q_{13}+(1-\alpha_2)Q_{23}}{h_c S} \\ + \frac{2(1-\alpha_1)Q_{13}r_{j1}}{A_{r1}K_3\sqrt{\pi(1.273+Pe_1)}} \tag{26}$$

$$\frac{\alpha_2 Q_{23}}{\pi r^2}\frac{l}{K_2} + \frac{\alpha_2 Q_{23}r_{j2}}{A_{r2}K_2} = \frac{(1-\alpha_1)Q_{13}+(1-\alpha_2)Q_{23}}{h_c S} \\ + \frac{2(1-\alpha_2)Q_{23}r_{j2}}{A_{r2}K_3\sqrt{\pi(1.273+Pe_2)}} \tag{27}$$

This determines the heat partitioning fraction and the T_c in both regions of contact.

It should be noted that this analytical model was deduced on the assumption that several separate

polymer contact asperities are sliding over a plane steel surface. Therefore, the polymer asperities can be considered to be subjected to a stationary heat source, while the steel plane is subject to a moving circular heat source. This also assumes that the steel has almost no deformation due to the large difference in *H*. However, this may lead to errors when a friction pair is with similar *H*, because both components will be deformed by each other. To address this issue, Smith and Arnell [54] and Lee et al. [55] explored a model that considers the interactions between individual contacting asperities. The resulting model was then further improved by Liu and Barber [56] and Lee et al. [57] by including the statistics of rough surface interactions during sliding, thereby making the contact process stochastic in both time and space. Their results revealed the effects of *Ra* and sliding speed upon the thermal contact resistance under very short sliding duration before approaching a thermal steady state. This asperity–asperity model may produce more accurate predictions relating to the contact conditions and temperature. In addition, it should be noted that the treatment of the actual contact asperities as strictly circular regions of equal area is another source of inaccuracy in the present study because, in reality, the actual contact areas generally have complex and individually distinct shapes. Finally, the meaningfulness of the calculated temperatures will be impacted if the adjacent contact regions are close enough to interact with each other.

3 Application

3.1 Experimental details

3.1.1 Preparation of test materials

The materials of the two pin specimens for the dual-pins-on-disk experiments were pure PEEK and PTFE/bronze composite. The PEEK was selected as a load-bearing component in the hybrid wear system due to its excellent mechanical and machinability properties [58]. The PEEK pins with diameters of 5 mm and lengths of 15 mm were lathed from a pure PEEK (Victrex, 450G, UK) bar stock.

The PTFE/bronze composite (Daikin, M-18F, Japan) was used as an independent lubricating component

in order to improve the tribological performance of the hybrid wear system due to its excellent tribofilm generating capability [59, 60]. The particle sizes of the PTFE and bronze particles were approximately 25 and 30–50 μm, respectively, according to the information provided by the manufacturers. The powders with 40 wt% bronze and 60 wt% PTFE were first mixed using a high-speed mixer, and then cold compressed under 60 MPa before being sintered at 370 °C for 3 h. Finally, the obtained PTFE composite rods were lathed into specimen pins with diameters and lengths of 5 and 15 mm, respectively.

The steel test ring, with a diameter of 54 mm and a height of 10 mm, was composed of bearing steel (GCr15, GB/T18254-2002). Its axial surface, with *Ra* ≈ 0.5 μm, was produced using a flat grinding process. The detailed physical properties of the selected materials are listed in Table 1. The thermal property data were provided by the suppliers, and the *H* values were measured as part of the present work using a Vickers hardness tester (Future-Tech Corp., FLC-50V, Japan). All of the values listed relate to room temperature conditions and are assumed to be constant during the temperature calculations.

3.1.2 Test conditions

As shown in Fig. 2, the experiments were conducted on a dual-pin-on-disk tribometer incorporating two independent loading/measuring devices. This apparatus allows the two specimen pins to be separately loaded against the test ring surface with different loads and their friction coefficients to be recorded separately in real time. The specific dimensional parameters of this apparatus are listed in Table 2, and a more detailed

Table 1 Physical properties of the materials used in the present study.

Property	PEEK (Pin (1))	PTFE composite (Pin (2))	GCr15 (Steel ring (3))
Thermal conductivity K (W/(m·°C))	0.29	1.07	46.06
H (MPa)	246.80	37.04	6,860
Thermal diffusivity κ (m²/s)	—	—	1.28×10^{-5}
Glass transition temperature T_g (°C)	150	116	—
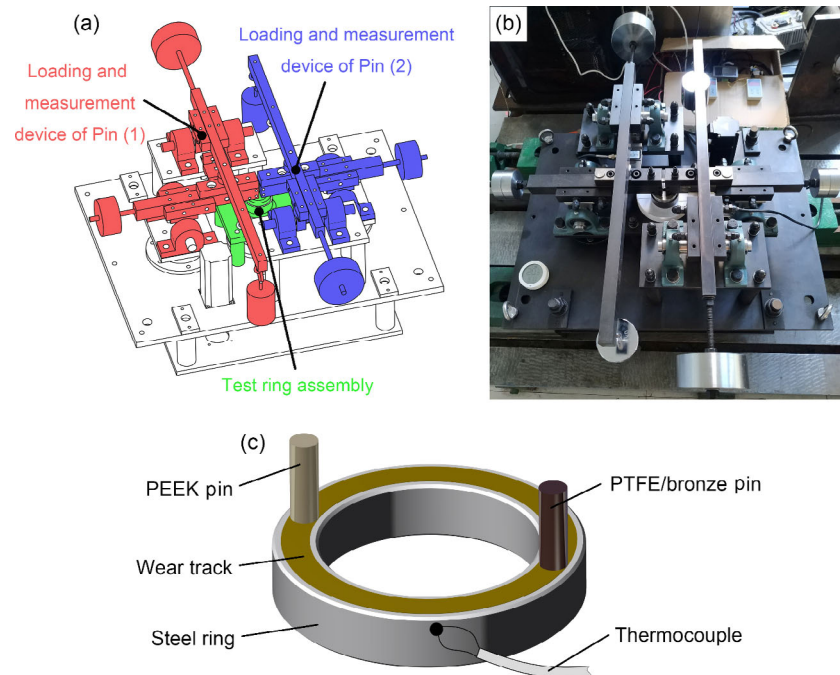
Fig. 2 (a) Schematic diagram and (b) photographic image of the dual-pin-on-disk test apparatus. (c) Schematic diagram of the the PEEK and PTFE/bronze dual-pin-on-disk friction pair, showing the measurement position of the thermocouple.

Table 2 Dimensional parameters of the dual-pin-on-disk test apparatus.

Parameter	Value
r (m)	5.0×10^{-3}
l (m)	1.5×10^{-2}
R (m)	2.3×10^{-2}
d (m)	5.4×10^{-2}
S (m^2)	3.77×10^{-2}
w (rad/s)	34.906

description of the device has been previously published [15]. Additionally, due to their good accuracy, thermocouples were used to measure the actual temperature of the wear track *in situ*. The thermocouple was affixed to the edge of the sliding face of the test ring and allowed to rotate synchronously with the test ring assembly (Fig. 2(c)). During the test, the electrical temperature signal was transmitted in real time to the signal receiver through a slip ring equipped with an electric brush. It should be noted that the measured temperature is considered to reflect ΔT_{n3} rather than ΔT_{c}, because ΔT_{f} only occurs at the micro-scale real contact region and dissipates quickly before being detected.

The experiments were conducted at room temperature under dry conditions (~19 °C, ~40% relative humidity). To obtain a uniform load distribution, both the PEEK and PTFE pins were pre-worn against sandpaper (Starcke, P600, Germany) at 0.1 m/s under a pressure of 0.2 MPa for 20 m sliding distance L prior to the wear test. To obtain a good balance between the wear rate of the PTFE composite and the PEEK, the load applied to the PTFE/bronze composite pin (F_{PTFE}) was fixed at 19.6 N (the nominal contact pressure P_{PTFE} = 1 MPa) in accordance with the previous work [15]. To investigate the load-carrying capacity of the hybrid wear system, along with the effect of contact temperature, the PEEK pin as the load-carrying component was subjected to various loads (F_{PEEK}) in the range of 39.2–137.2 N, corresponding to a P_{PEEK} of 2–7 MPa. The sliding speed and L were fixed at 0.8 m/s and 15 km, respectively. Each test condition was repeated at least three times, and fresh samples were used in every test.

The average values of the friction coefficients of the pure PEEK and of the PTFE composite during the entire steady-state period (3–15 km) were calculated as the steady-state friction coefficients under each test condition. To obtain the wear mass loss, the weights

of the pin specimens before and after the wear test were measured using an electronic analytical balance (Sartorius, Germany) with an accuracy of 0.01 mg. The specific wear rates of the PEEK W_{PEEK} (mm³/(N·m)) and the PTFE composite W_{PTFE} (mm³/(N·m)) were calculated as the material volume loss Δm under each load F (N) and L (m) according to Eq. (28):

$$W = \frac{\Delta m}{\rho F L} \quad \text{(mm}^3\text{/(N·m))} \tag{28}$$

where ρ is the density of the pure PEEK or the PTFE/bronze composite specimen, and L = 15 km.

After the wear tests, the worn surfaces of the PEEK, PTFE composite, and steel ring were observed using the optical microscopy and field-emission scanning electron microscope (SEM; FEI, Nova Nano 450, USA) to observe the formation of tribofilms and morphologies of worn surface to analyze the wear mechanism. Furthermore, the energy dispersive spectrometer incorporated into SEM was used to analyze the elemental compositions and the origin of the tribofilms. The Fourier transform infrared (FTIR) spectroscopy data of the transfer films were attained using an attenuated total reflectance (ATR; Thermo Scientific, Nicolet iS10, USA) to analyze the tribo-chemistry reactions.
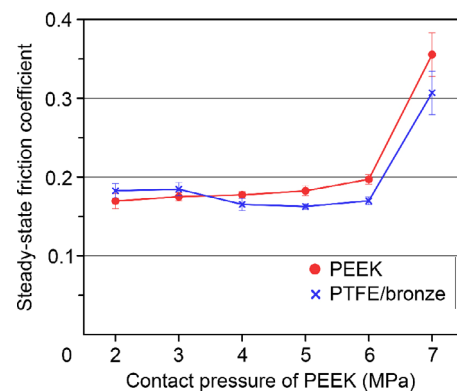
3.2 Friction and wear results

The steady-state friction coefficients of the pure PEEK and the PTFE/bronze composite under hybrid wear conditions with various P_{PEEK} values are presented in Fig. 3. Here, when the P_{PEEK} does not exceed 6 MPa, the friction coefficient of the unfilled PEEK is seen to be significantly decreased from the well-established value of ~0.40 under single-pin-on-disk conditions [4, 15, 61], to 0.15–0.20 under the dual-pin-on-disk conditions. This indicates that the released PTFE composite debris that is retained in the wear track significantly improves the friction performance of the PEEK. When the P_{PEEK} is increased to 7 MPa, however, the friction coefficient of the PEEK is seen to suddenly increase to more than 0.35. Interestingly, the friction coefficient of the lubricant supplier PTFE composite is also increased to approximately 0.30 under this condition. These characteristics of the friction coefficient are closely related to the formation of tribofilms on the sliding

surfaces, which is described in detail in Section 3.4.

The evolution processes of the friction coefficients of the pure PEEK and of the PTFE composite with L are presented in Fig. 4. Here, when the P_{PEEK} does not exceed 4 MPa, the friction coefficient of the pure PEEK is seen to stabilize at less than 0.20 after a running-in stage of approximately 1.5 km. In detail, the friction coefficient of the pure PEEK initially increases due to the larger frictional force generated by the increased contact area because the sliding surfaces were slowly polished at the beginning of the experiment, and then decreases slowly with the gradual generation of the tribofilm. By contrast, when the P_{PEEK} is 5 or 6 MPa, the friction coefficient of the PEEK gradually increases but does not stabilize in the steady state condition, even though a similar running-in stage is observed during the initial 3 km of sliding. When the P_{PEEK} is further increased to 7 MPa, the friction coefficient of the PEEK is seen to increase rapidly from the beginning of the experiment to a level exceeding 0.35, after which dramatic fluctuations are observed throughout the experiment.
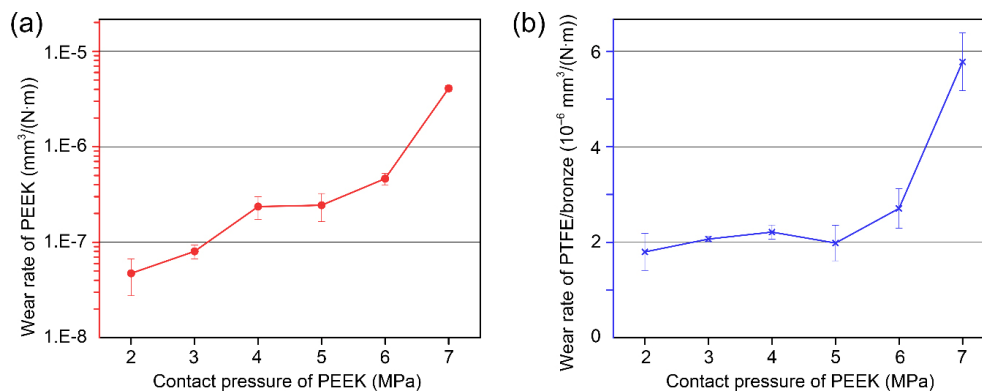
The wear rates of the pure PEEK and of the PTFE composite under various hybrid wear conditions are presented in Fig. 5. Here, when the P_{PEEK} is less than 6 MPa, the wear rate of the pure PEEK is seen to increase slightly with increased contact pressure. In detail, when the P_{PEEK} is 2 or 3 MPa, the wear rate of the PEEK is less than 10^{-7} mm³/(N·m), and this increases to 10^{-6}–10^{-7} mm³/(N·m) when the P_{PEEK} is increased to 4–6 MPa. This represents a significant improvement in the wear performance of the pure PEEK compared

Fig. 3 Steady-state friction coefficients of the PEEK and the PTFE/bronze composite as a function of the P_{PEEK} under hybrid wear conditions. The error bars represent the standard deviations of the results of repeated experiments under each test condition.
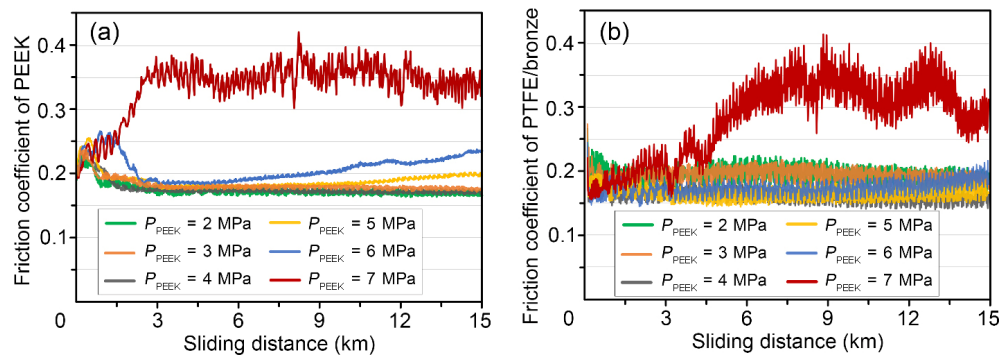
Fig. 4 Friction coefficients of (a) the PEEK and (b) the PTFE/bronze composite vs. sliding distance under hybrid wear conditions with various contact pressures on the PEEK.

Fig. 5 Specific wear rates of (a) the PEEK and (b) the PTFE/bronze composite as a function of the P_{PEEK} under hybrid wear conditions. The error bars represent the standard deviations of the results of repeated experiments under each test condition.

with that obtained under the single-pin-on-disk condition (i.e., ~10^{-5} mm^3/(N·m)) [4, 15, 61]. However, the wear rate of the PEEK is seen to deteriorate dramatically by one order of magnitude (to more than 10^{-6} mm^3/(N·m)) when the P_{PEEK} is increased to 7 MPa. The wear rate of the PTFE composite is also increased by more than two times under this condition, although the contact pressure was constant.

3.3 Temperature results

3.3.1 Contact temperature calculation

The measured temperatures and the corresponding calculated temperatures obtained by the analytical method are presented in Fig. 6 and Table 3. The processes for determining the heat convection coefficient (h_c) and the radius of a individual actual contact asperity (r_j) are detailed in Appendixes A and B, respectively. It should be noted that the accuracy of the temperature calculation is greatly affected by these two parameters. Therefore, their estimation should not be limited to

the methodology presented herein; later, different methods should be selected according to the specific working conditions. The analytical method used herein suggests that the temperature measured by the thermocouple positioned at the edge of the steel face should be comparable to $T_{amb} + \Delta T_{n3}$ under each working condition. ΔT_f cannot be detected by the thermocouple because it disappears quickly within the micro-contact area. Indeed, the results of the measured temperature (marked as crosses in Fig. 6) agree well with the calculated $T_{amb} + \Delta T_{n3}$ (the yellow and orange bars in Fig. 6), and the errors are within 10% (Table 3), thereby demonstrating the good accuracy of the analytical method for predicting the contact temperature of the hybrid wear system.

It should be noted that the properties used for temperature calculation are the values obtained under room-temperature conditions and are assumed to be constant and uniform. In fact, the material properties data (e.g., K and H) could be significantly different at elevated temperature. Hence, the use of temperature-
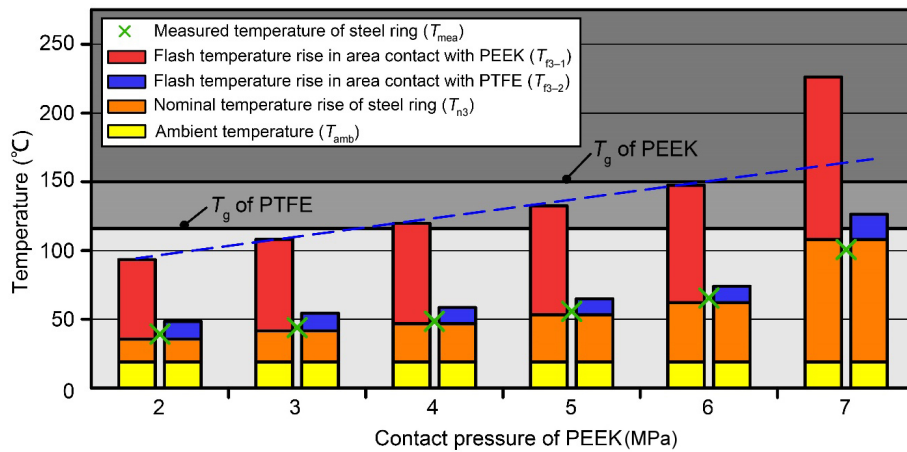
Fig. 6 Measured and analytical temperatures of the steel ring surface in contact with the pure PEEK (left-hand bar in each pair) and in contact with the PTFE (right-hand bar in each pair) under hybrid wear conditions with varied P_{PEEK}. The blue dashed line indicates the trend of the T_c of the sliding surface when the P_{PEEK} is below 6 MPa.

Table 3 Measured and calculated contact temperatures.

Loading condition	ΔT_{n3} (°C)	ΔT_{f3-1} (°C)	ΔT_{f3-2} (°C)	T_{c3-1} (°C)	T_{c3-2} (°C)	$T_{amb} + \Delta T_{n3}$ (°C)	T_{mea} (°C)	Error
2 MPa PEEK + 1 MPa PTFE	16.59	**57**.80	12.79	93.39	48.39	35.59	39.17	9.1%
3 MPa PEEK + 1 MPa PTFE	22.58	66.54	12.89	108.12	54.47	41.58	43.93	5.4%
4 MPa PEEK + 1 MPa PTFE	27.84	72.88	11.75	119.72	58.59	46.84	48.53	3.5%
5 MPa PEEK + 1 MPa PTFE	34.24	79.27	11.61	132.51	64.85	53.24	55.77	4.5%
6 MPa PEEK + 1 MPa PTFE	43.04	85.40	11.99	147.44	74.03	62.04	65.40	5.1%
7 MPa PEEK + 1 MPa PTFE	89.03	118.20	18.28	226.23	126.31	108.03	100.70	7.3%

dependent material properties may further increase the accuracy of the prediction. The K of the polymer does not vary significantly over the temperature range explored in the present study [62, 63]. Mu et al. [64] also shows that the change in K is not the major influence on the contact temperature. However, the elevated temperature could cause a distinct softening of the polymer, thereby significantly decreasing its hardness. As a result, higher analytical flash temperatures may be predicted because the calculated contact areas are smaller than the actual ones, especially under high-load and high-temperature conditions. Furthermore, the polymer tribofilms formed on the sliding surfaces also affect the thermal behavior of the contact region when a F-based transfer film with lower K covers the surface of the steel ring (Section 3.4). This tends to prevent the heat from entering the steel substrate, thereby providing less heat for maintaining the steady state temperature. This, in turn, leads to an over-estimation of the steady-state temperature by the analytical model that ignores the effects of tribofilms.

3.3.2 Contact temperature analysis

The orange bars in Fig. 6 indicate that under each loading condition, the ΔT_n of the steel ring surface is constant, but different T_c occur at the contacts with the PEEK (the red bars) and the PTFE (the blue bars) composites due to the different ΔT_f. The contact region between the steel ring and the PEEK component tends to exhibit a higher T_c because the applied load on the PEEK component is higher than that on the PTFE; hence, more heat is generated within the former contact region. When the P_{PEEK} remains below 6 MPa, the T_c of the PEEK and the PTFE composite increases approximately linearly with the P_{PEEK} (the blue dashed line, Fig. 6) because the steady-state friction coefficients of both materials are almost constant under these conditions (Fig. 3) and hence,

the heat generated is approximately proportional to the P_{PEEK}. It should also be noted that the T_c of the PEEK exceeds the T_g of PTFE (~116 °C [65]) when the P_{PEEK} exceeds 4 MPa. When the P_{PEEK} reaches 7 MPa, however, the sudden increase in friction coefficient of the two components (Fig. 3) increases the generated heat significantly, thus resulting in a remarkable increase in T_c. Under this condition, the T_{c3-1} of the steel ring at the region of contact with the PEEK component will exceed the T_g of PEEK (~150 °C), and the T_{c3-2} of the region in contact with the PTFE component will exceed the T_g of PTFE (~116 °C). This may be the core reason for the significant change in the tribological performance of the hybrid wear system under 7 MPa test conditions (Section 3.4).

3.4 Worn surface analyses

The morphologies of the worn surfaces of the polymer specimens and of the counterpart steel rings

were observed in order to study the formation of tribofilms, and the results were linked to the temperature observations to explore the failure mechanism of the hybrid wear system under high load conditions (i.e., 7 MPa). The SEM morphologies of the PEEK worn surfaces and their corresponding energy dispersive X-ray spectrometry (EDS) results under the various test conditions are presented in Figs. 7 and 8, while the typically worn surfaces of the steel ring and the PTFE composite are shown in Fig. 9.

A high-quality secondary transfer film that approximately covers the entire PEEK worn surface can be seen when the contact pressure is 2 or 3 MPa (Figs. 7(a) and 7(b)). Further, the EDS results show that a significant amount of F and Cu are present on the worn surface of the PEEK under both conditions (Fig. 8), thereby indicating that the primary source of the secondary transfer film is the PTFE/bronze composite. As shown in Fig. 9(a), a transfer film with
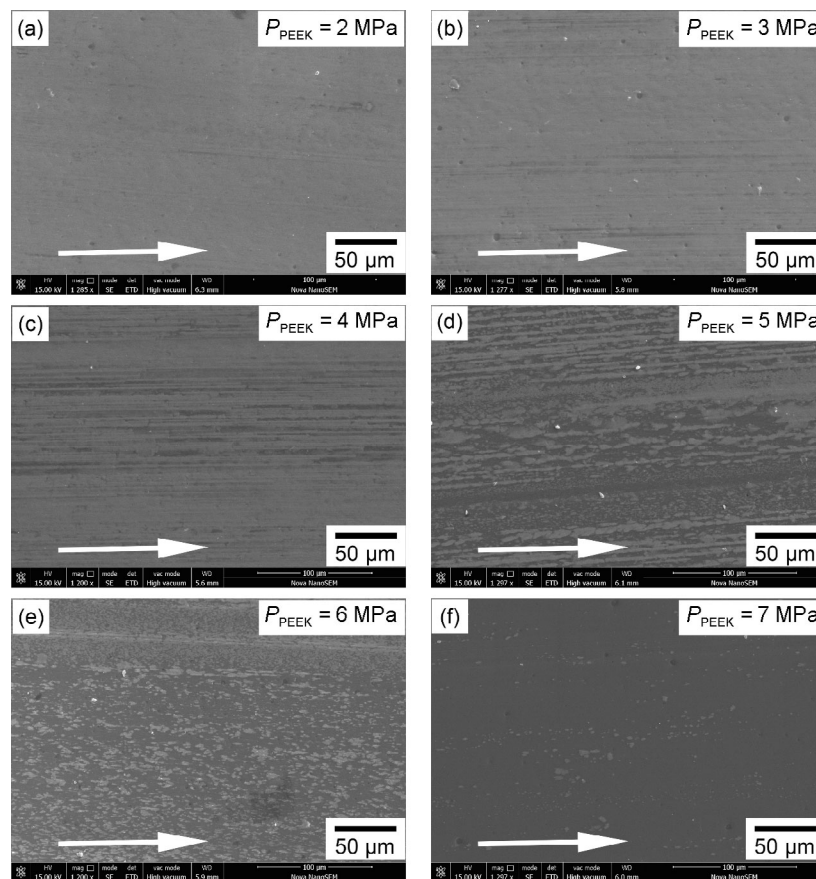

Fig. 7 SEM micrographs of the worn PEEK surfaces after sliding against the steel ring under contact pressures of (a) 2 MPa, (b) 3 MPa, (c) 4 MPa, (d) 5 MPa, (e) 6 MPa, and (f) 7 MPa in the hybrid wear setup incorporating the PTFE composite. The white arrows indicate the sliding direction.
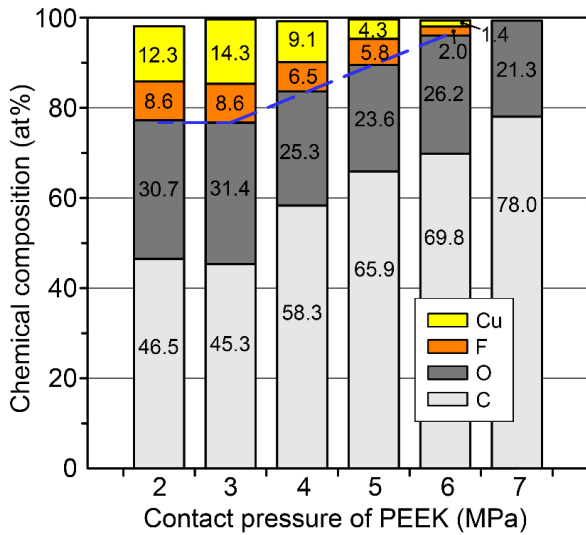
Fig. 8 EDS chemical analysis of the worn PEEK surfaces after the hybrid wear tests with varied P_{PEEK}. The dashed blue line shows the trend in the sum of Cu and F contents, which indicates the coverage of the specimen with the F-based tribofilm.

good coverage is also generated on the worn surface of the steel ring under this condition. Here, the plateaus of the steel surface are well covered by the transfer film, thus indicating that the steel asperities could not directly abrade the polymer surface during the sliding process. Meanwhile, no exposed bronze particles are observed on the corresponding worn PTFE surface (Fig. 9(b)), and a running film with large coverage is observed. These results indicate that the wear debris released by the PTFE composite into the hybrid wear track can generate tribofilms on the surfaces of the PEEK pin, the PTFE composite pin, and the test ring after being repeatedly crushed and sheared during the test. The process of sliding between the polymer component and the steel ring was then transformed to one of sliding between the F-based tribofilms, thus resulting in a low friction coefficient and wear rate of the PEEK component.
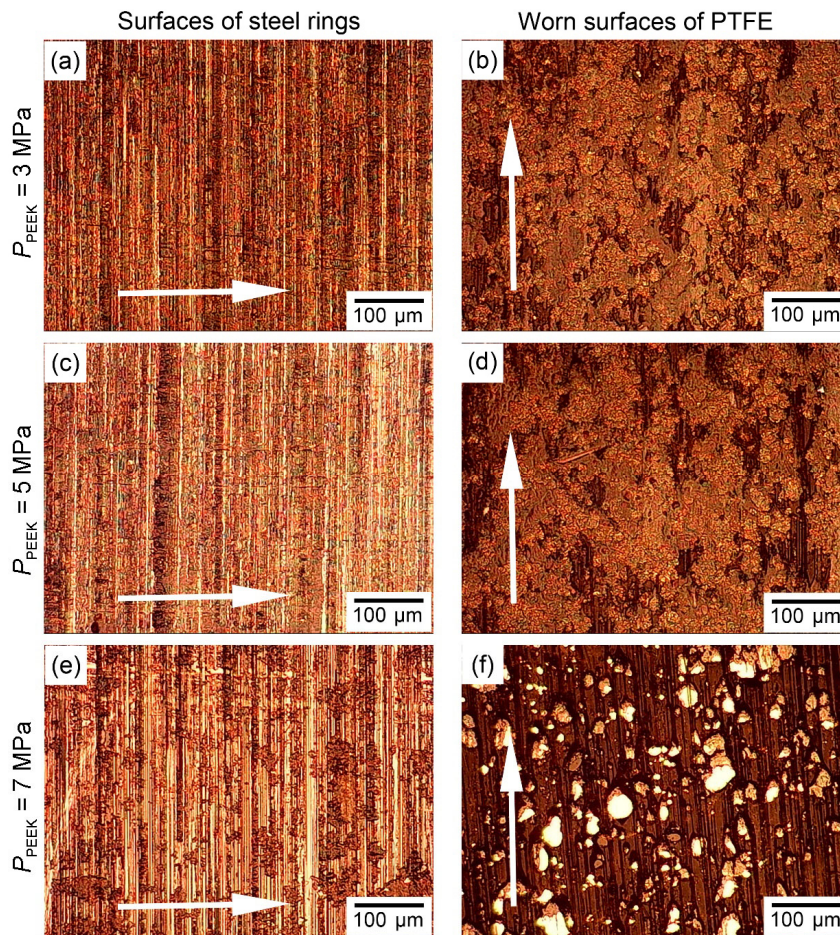
Fig. 9 Optical microscope images of the worn surfaces of the steel ring and the PTFE/bronze composite after the hybrid wear tests with P_{PEEK} values of (a, b) 3 MPa, (c, d) 5 MPa, and (e, f) 7 MPa. The white arrows indicate the sliding direction.

These results agree well with the previous work by the same authors [15]. The similar source of frictional force on the pure PEEK and the PTFE composite also explains their similar steady-state friction coefficients (Fig. 3). Moreover, the hard PEEK matrix leads to a smaller contact area than that of the PTFE component, thereby resulting in a slightly smaller friction coefficient of the PEEK component.

When the P_{PEEK} is in the range of 4–6 MPa, however, some distinct dark areas representing exposed PEEK matrix can be seen in the SEM images of the worn PEEK surfaces (Figs. 7(c)–7(e)). The exposed PEEK substrate appears dark due to its lower mean electron density than that of the bronze-containing secondary transfer film. This indicates the partial loss and flaking of the secondary transfer film under these conditions, and the coverage of the secondary transfer film decreases with increasing P_{PEEK}. This is confirmed by the EDS results in Fig. 8, where the contents of elements F and Cu are seen to decrease gradually with increasing P_{PEEK}. This occurs because an increase in the load leads to an increase in the contact temperature such that the peak temperature of the wear track (T_{c3-1}) exceeds the T_g of the PTFE (Fig. 6). This, in turn, results in a decrease in the mechanical strength of the F-based secondary transfer film such that wear and flaking can occur under the increased shear forces caused by the high contact pressure. This also explains why the friction coefficient of the PEEK increases slightly in the later stages of the experiment (Fig. 4) and becomes slightly greater than that of the PTFE component (Fig. 3) under these conditions. Nevertheless, transfer films and running films with good coverage are still formed on the worn surfaces of the test ring and the PTFE composite under these conditions (Figs. 9(c) and 9(d)) because the contact temperature between the steel ring and the PTFE component (i.e., T_{c3-2}) is still below the T_g of PTFE (Fig. 6). This indicates that the friction and wear process are still dominated by the sliding between the F-based tribofilms. Hence, the PEEK retains a friction coefficient of less than 0.25 and a wear rate of less than 10^{-6} mm^3/(N·m).

When the P_{PEEK} is increased to 7 MPa, qualitative changes in the morphologies of the worn surfaces are observed. Thus, the PEEK substrate is completely exposed without any coverage by an F-based secondary transfer film (Fig. 7(f)), as confirmed by the virtual absence of F and Cu in the EDS results under this operating condition (Fig. 8). Moreover, as shown in Fig. 9(e), a transfer film is deposited in the valleys of the steel surface without covering any of the plateau areas. As a result, the exposed asperities of the steel surface were able to directly scrape the PEEK surface during the sliding process, thereby accounting for the ultra-high friction coefficient and wear rate of the PEEK component. Furthermore, the running film formed on the PTFE composite surface has also disappeared, and the exposed bronze particles can be observed (Fig. 9(f)). These results demonstrate that the tribofilm formation process is completely hindered under the high loading condition, and this is believed to be closely related to the contact temperature condition.

3.5 Mechanism

When the P_{PEEK} is 7 MPa, the results in Section 3.3 indicate that the peak temperature at the contact region between the PEEK pin and the steel ring (i.e., T_{c3-1}) significantly exceeds the T_g of PEEK (~150 °C) due to the dramatic increase in the friction coefficient. However, the T_{c3-1} was also found to exceed the T_g of PEEK even though there was no dramatic increase in the friction coefficient (the blue dashed line in Fig. 6). Therefore, as shown in Fig. 10, certain conjectures can be made about the failure mechanism of the hybrid wear system under the 7-MPa operating condition. Thus, at a moderate contact temperature, the hybrid wear system exhibits the good tribological performance due to the formation of tribofilms (Fig. 10(a)). However, as the temperature field builds up due to the heat accumulated in the bodies of the sliding components, the peak temperature of the micro-scale actual contact area between the PEEK component and the steel ring (T_{c3-1}) first exceeds the T_g of the PTFE (116 °C) and then that of the PEEK (150 °C) (Fig. 10(b)). This leads to the softening of both the PTFE composite debris within this contact region and the PEEK sliding surface. As a result, the composite debris cannot be retained on the PEEK surface to generate a tribofilm and hence, direct contact occurs between the PEEK surface and the exposed steel spikes, thereby raising the friction coefficient of
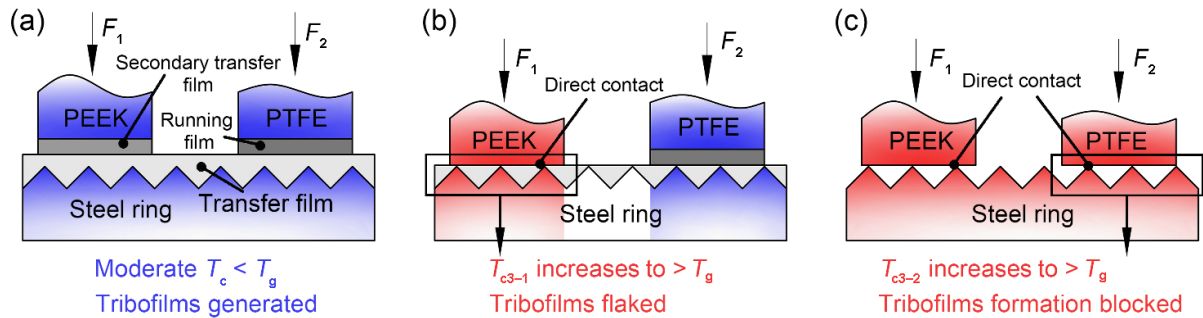
Fig. 10 Schematic diagrams of the failure mechanism of the hybrid wear system under high-load operating conditions.

the PEEK above 0.3. This, in turn, increases the heat entering the wear track, thereby further increasing the nominal temperature of the wear track and completely blocking the generation of F-based tribofilms on the surfaces of the steel ring and the PEEK. The deteriorating temperature field then affects the contact region between the PTFE component and the steel ring via the elevated nominal temperature of the shared wear track (Fig. 10(c)). This causes the T_c of the PTFE component to exceed the T_g of PTFE (Fig. 6) and hinders the formation of a running film on the worn PTFE surface. Consequently, direct contact is established between the exposed PTFE surface and the steel asperities, thereby accounting for the increase in the friction coefficient and wear rate of the PTFE component. The plowing marks observed on the PTFE worn surface running parallel to the sliding direction in Fig. 9(f) demonstrate the 2D abrasive wear caused by the exposed steel spikes.

The attenuated total reflection-Fourier transform infrared (ATR-FTIR) spectra of the transfer films formed on the steel ring during the hybrid wear tests are presented in Fig. 11. Here, the presence of $-CF_2-$ is clearly demonstrated by the absorption peaks at 1,154 and 1,210 cm^{-1} [66, 67] when the contact pressure of the PEEK is between 2 and 6 MPa. However, the characteristic absorption peaks of the PEEK phenyl ring vibrations at 1,594 and 1,489 cm^{-1} [68, 69] are not detected under these conditions. This confirms that the main component of the transfer film is PTFE rather than PEEK when the P_{PEEK} does not exceed 6 MPa. In addition, the absorption peaks are observed at 1,659 and 1,410 cm^{-1} under these conditions, corresponding to the vibration of the carboxylate ($-COO^-$) groups [70, 71]. Considering the absence of PEEK under this condition and the pure PTFE did not show these peaks,

so their appearance can be confidently attributed to the occurrence of tribo-chemical reactions. This reveals that the C–C bonds of the PTFE chain that are broken due to shearing will allow reaction with water vapor from the environment to produce carboxylate acid chain ends, which then become chelated to the surfaces of the steel ring and the bronze filler particles [72, 73]. This results in the formation of robust, adherent, and hardened triboflms on the sliding surfaces, as revealed in Fig. 9.

In Fig. 11, when the P_{PEEK} is increased to 7 MPa, the typical PTFE peaks at 1,154 and 1,210 cm^{-1} are seen to have disappeared, and those of the carbonyl stretching vibrations, phenyl ring vibrations, and aromatic ether group stretching vibrations of the PEEK can be observed at 1,648, 1,594 and 1,489, and 1,220 cm^{-1}, respectively [68, 69]. This observation indicates that the PTFE transfer film is extruded out from the wear track due to the high contact temperature under the high loading condition, and that the PEEK then takes
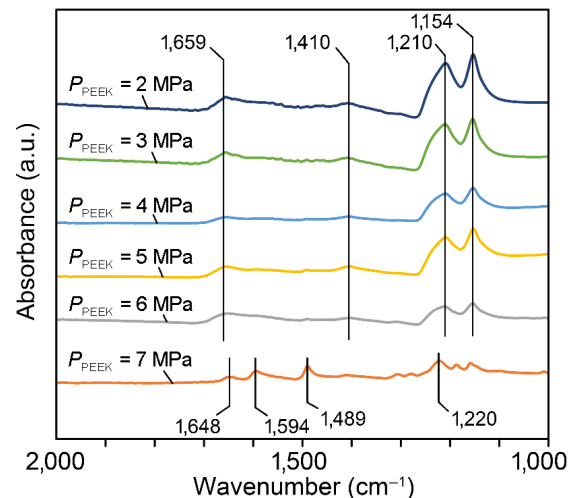
Fig. 11 ATR-FTIR spectra of the transfer films formed on the steel ring surface during the hybrid wear tests with varied P_{PEEK}.

over as the primary source of the transfer film. This leads to a deterioration in the tribological performance of the hybrid wear system.

4 Conclusions

1) An analytical method was developed herein to predict the contact temperature of a dual-pin-on-disk hybrid wear system. The accuracy of the theoretical model was demonstrated by the experimental results.

2) The heat generated by the various components played a limited synergistic role in the hybrid wear system. The nominal temperature rise ΔT_n of the shared wear track was determined by the heat generated by all components, whereas the local flash temperature rise was dependent upon the individual characteristics of each component.

3) Different peak temperature T_c were shown to exist in the same wear track at regions in contact with different components of the hybrid wear system, and the tribological performance of the system was shown to depend upon the overall highest T_c.

4) When the applied load on the PEEK–PTFE–steel hybrid wear system was sufficiently high for T_c to exceed glass transition temperature T_g of both polymer pin components, tribofilms were unable to form on the sliding surfaces and hence, the hybrid wear system failed. Conversely, when the P_{PEEK} was less than 6 MPa, robust, adherent, and hardened tribofilms were formed on the sliding surfaces, and the tribological performance was enhanced compared to that of the single-pin-on-disk setup.

Acknowledgements

Appendix A Heat convection coefficient h_c

To simplify and increase the general applicability of the model, the rotating test ring assembly was converted into an equivalent disk [23] with area S and rotation speed w. It was also assumed that the surface temperature of the equivalent disk is uniform and equal to that of the test ring (i.e., $T_{amb} + \Delta T_{n3}$). Kreith et al. [50] concluded that the average Nusselt number Nu_D and the Reynolds number Re_w of a disk rotating under an atmosphere of air in the laminar flow regime are given by Eqs. (A1) and (A2):

$$Nu_D = \frac{h_c D}{K_a} = 0.36\sqrt{Re_w} \qquad (A1)$$

$$Re_w = \frac{wD^2}{v_a} < 10^6 \qquad (A2)$$

where D is the diameter of the equivalent disk ($D = 2\sqrt{S/\pi}$), and K_a and v_a are the thermal conductivity and viscosity of the air, respectively. Under room-temperature conditions, the values of K_a and v_a are approximately 0.025 W/(m·°C) and 1.6×10⁻⁵ m²/s, respectively. Substituting these values into Eqs. (A1) and (A2) gives h_c = 13.29 W/(m²·°C).

Appendix B Radius of the actual contact area r_j

The micro-contact area of the sliding surface often suffers a complex mixture of elastic and plastic deformation. This is influenced by various factors such as Ra, loading conditions, and material properties. A generalized theoretical model for calculating the actual micro-scale contact area does not yet exist. In the present work, because the H of the polymer pins are considerably less than that of the steel test rings, it is assumed that the deformation of the polymer pin is entirely plastic, and that the pressure is equal to the maximum that can be sustained by the softer pin. The empirical formula introduced by Ashby et al. [35] and Tabor [36], along with the modified analytical equations of Wang and Rodkiewicz [28], were adopted in order to predict the actual contact area A_r and radius of each asperity in the contact region r_j as Eqs. (A3)–(A5):

$$A_r = \frac{F_i\sqrt{1+12\mu_i^2}}{H_i} \qquad (A3)$$

$$r_j = \sqrt{\frac{A_r}{\pi}}, \quad A_r < \pi r_a^2 \qquad (A4)$$

$$r_j = r\left[\left(1-\frac{F}{F_s}\right)\left(\frac{r}{r_a}\right)^2 + 1\right]^{-1/2}, \quad A_r > \pi r_a^2 \qquad (A5)$$

where H_i is the hardness of the softer material of the two surfaces (i.e., the hardness of Pin (i) (Table 1)). The seizure load F_s is given by $F_s = \dfrac{\pi r_a^2 H_i}{\sqrt{1+12\mu_i^2}}$, where $r_a = \dfrac{0.1}{H_i}$, is the load-independent radius of a unit asperity.

References

[1] Zorko D, Kulovec S, Duhovnik J, Tavčar J. Durability and design parameters of a steel/PEEK gear pair. *Mech Mach Theory* **140**: 825–846 (2019)

[2] Fusaro R L. Self-lubricating polymer composites and polymer transfer film lubrication for space applications. *Tribol Int* **23**(2): 105–122 (1990)

[3] Shen M X, Li B, Ji D H, He X R, Lin X Z, Xiong G Y. Effect of contact stress on the tribology behaviors of PTFE/316L seal pairs under various abrasive-contained conditions. *Proc Inst Mech Eng Part J J Eng Tribol* **235**(3): 639–652 (2021)

[4] Zalaznik M, Kalin M, Novak S. Influence of the processing temperature on the tribological and mechanical properties of poly-ether-ether-ketone (PEEK) polymer. *Tribol Int* **94**: 92–97 (2016)

[5] Valente C A G S, Boutin F F, Rocha L P C, do Vale J L, da Silva C H. Effect of graphite and bronze fillers on PTFE tribological behavior: A commercial materials evaluation. *Tribol Trans* **63**(2): 356–370 (2020)

[6] Rodriguez V, Sukumaran J, Schlarb A K, de Baets P. Influence of solid lubricants on tribological properties of polyetheretherketone (PEEK). *Tribol Int* **103**: 45–57 (2016)

[7] Burris D L, Sawyer W G. A low friction and ultra low wear rate PEEK/PTFE composite. *Wear* **261**(3–4): 410–418 (2006)

[8] Guo L H, Qi H M, Zhang G, Wang T M, Wang Q H. Distinct tribological mechanisms of various oxide nanoparticles added in PEEK composite reinforced with carbon fibers. *Compos A Appl Sci Manuf* **97**: 19–30 (2017)

[9] Bhargava S, Blanchet T A. Unusually effective nanofiller a contradiction of microfiller-specific mechanisms of PTFE composite wear resistance? *J Tribol* **138**(4): 042001 (2016)

[10] Bijwe J, Sen S, Ghosh A. Influence of PTFE content in PEEK–PTFE blends on mechanical properties and tribo-performance in various wear modes. *Wear* **258**(10): 1536–1542 (2005)

[11] Vaganov G, Yudin V, Vuorinen J, Molchanov E. Influence of multiwalled carbon nanotubes on the processing behavior of epoxy powder compositions and on the mechanical properties of their fiber reinforced composites. *Polym Compos* **37**(8): 2377–2383 (2016)

[12] Lu Z P, Friedrich K. On sliding friction and wear of PEEK and its composites. *Wear* **181–183**: 624–631 (1995)

[13] Li G T, Qi H M, Zhang G, Zhao F Y, Wang T M, Wang Q H. Significant friction and wear reduction by assembling two individual PEEK composites with specific functionalities. *Mater Des* **116**: 152–159 (2017)

[14] Lin L Y, Ecke N, Huang M Z, Pei X Q, Schlarb A K. Impact of nanosilica on the friction and wear of a PEEK/CF composite coating manufactured by fused deposition modeling (FDM). *Compos B Eng* **177**: 107428 (2019)

[15] Lin Z B, Yue H Q, Gao B Z. Enhancing tribological characteristics of PEEK by using PTFE composite as a sacrificial tribofilm-generating part in a novel dual-pins-on-disk tribometer. *Wear* **460–461**: 203472 (2020)

[16] Lin Z B, Zhang K, Ye J X, Li X J, Zhao X G, Qu T, Liu Q F, Gao B Z. The effects of filler type on the friction and wear performance of PEEK and PTFE composites under hybrid wear conditions. *Wear* **490–491**: 204178 (2022)

[17] Balic E E, Blanchet T A. Transfer solid lubrication of aluminum sliding contacts. *Tribol Trans* **51**(3): 265–270 (2008)

[18] McC Ettles C M, Shen J H. The influence of frictional heating on the sliding friction of elastomers and polymers. *Rubber Chem Technol* **61**(1): 119–136 (1988)

[19] Jean-Fulcrand A, Masen M A, Bremner T, Wong J S S. Effect of temperature on tribological performance of polyetheretherketone-polybenzimidazole blend. *Tribol Int* **129**: 5–15 (2019)

[20] Friedrich K, Karger-Kocsis J, Lu Z. Effects of steel counterface roughness and temperature on the friction and wear of PE(E)K composites under dry sliding conditions. *Wear* **148**(2): 235–247 (1991)

[21] Seshadri I, Esquenazi G L, Borca-Tasciuc T, Keblinski P, Ramanath G. Multifold increases in thermal conductivity of polymer nanocomposites through microwave welding of metal nanowire fillers. *Adv Mater Interfaces* **2**(15): 1500186 (2015)

[22] Tian X, Kennedy F E, Deacutis J J, Henning A K. The development and use of thin film thermocouples for contact temperature measurement. *Tribol Trans* **35**(3): 491–499 (1992)

[23] Shi Y, Yao Y P. Temperature field analysis of pin-on-disk sliding friction test. *Int J Heat Mass Transf* **107**: 339–346 (2017)

[24] Kennedy Jr F E. Surface temperatures in sliding systems—A finite element analysis. *J Lubr Technol* **103**(1): 90–96 (1981)

[25] Kennedy F E, Lu Y, Baker I. Contact temperatures and their influence on wear during pin-on-disk tribotesting. *Tribol Int* **82**: 534–542 (2015)

[26] Rahaman M L, Zhang L C. On the estimation of interface temperature during contact sliding of bulk metallic glass. *Wear* **320**: 77–86 (2014)

[27] Singh R A, Narasimham G S V L, Biswas S K. Estimation of surface temperature of a pin wearing on a disk. *Tribol Lett* **12**(4): 203–207 (2002)

[28] Wang Y, Rodkiewicz C M. Temperature maps for pin-on-disk configuration in dry sliding. *Tribol Int* **27**(4): 259–266 (1994)

[29] Dyson J, Hirst W. The true contact area between solids. *Proc Phys Soc B* **67**(4): 309 (1954)

[30] O'callaghan P W, Probert S D. Prediction and measurement of true areas of contact between solids. *Wear* **120**(1): 29–49 (1987)

[31] Wahl K J, Chromik R R, Lee G Y. Quantitative *in situ* measurement of transfer film thickness by a Newton's rings method. *Wear* **264**(7–8): 731–736 (2008)

[32] Greenwood J A, Williamson J B P. Contact of nominally flat surfaces. *P Roy Soc A Math Phys Eng Sci* **295**(1442): 300–319 (1966)

[33] McCool J I. Comparison of models for the contact of rough surfaces. *Wear* **107**(1): 37–60 (1986)

[34] Liu Z Q, Neville A, Reuben R L. A numerical calculation of the contact area and pressure of real surfaces in sliding wear. *J Tribol* **123**(1): 27–35 (2001)

[35] Ashby M F, Abulawi J, Kong H S. Temperature maps for frictional heating in dry sliding. *Tribol Trans* **34**(4): 577–587 (1991)

[36] Tabor D. Junction growth in metallic friction: The role of combined stresses and surface contamination. *P Roy Soc A Math Phys Eng Sci* **251**(1266): 378–393 (1959)

[37] Rowe K G, Bennett A I, Krick B A, Sawyer W G. *In situ* thermal measurements of sliding contacts. *Tribol Int* **62**: 208–214 (2013)

[38] Shakhvorostov D, Pöhlmann K, Scherge M. An energetic approach to friction, wear and temperature. *Wear* **257**(1–2): 124–130 (2004)

[39] Kennedy Jr F E. Thermal and thermomechanical effects in dry sliding. *Wear* **100**(1–3): 453–476 (1984)

[40] Tian X F, Kennedy Jr F E. Contact surface temperature models for finite bodies in dry and boundary lubricated sliding. *J Tribol* **115**(3): 411–418 (1993)

[41] Gecim B, Winer W O. Steady temperature in a rotating cylinder subject to surface heating and convective cooling. *J Tribol* **106**(1): 120–126 (1984)

[42] Liu S B, Lannou S, Wang Q, Keer L. Solutions for temperature rise in stationary/moving bodies caused by surface heating with surface convection. *J Heat Transf* **126**(5): 776–785 (2004)

[43] Kennedy F E, Frusescu D, Li J Y. Thin film thermocouple arrays for sliding surface temperature measurement. *Wear* **207**(1–2): 46–54 (1997)

[44] Laux K A, Jean-Fulcrand A, Sue H J, Bremner T, Wong J S S. The influence of surface properties on sliding contact temperature and friction for polyetheretherketone (PEEK). *Polymer* **103**: 397–404 (2016)

[45] Tzanakis I, Conte M, Hadfield M, Stolarski T A. Experimental and analytical thermal study of PTFE composite sliding against high carbon steel as a function of the surface roughness, sliding velocity and applied load. *Wear* **303**(1–2): 154–168 (2013)

[46] Kennedy F E, Tian X. Modeling sliding contact temperatures, including effects of surface roughness and convection. *J Tribol* **138**(4): 042101 (2016)

[47] Jaeger J C. Moving sources of heat and the temperature of sliding contacts. *Proc Roy Soc New South Wales* **76**(202) (1942)

[48] Laraqi N, Alilat N, de Maria J M G, Baïri A. Temperature and division of heat in a pin-on-disc frictional device—Exact analytical solution. *Wear* **266**(7–8): 765–770 (2009)

[49] Alilat N, Baïri A, Laraqi N. Three-dimensional calculation of temperature in a rotating disk subjected to an eccentric circular heat source and surface cooling. *Numer Heat Transf A Appl* **46**(2): 167–180 (2004)

[50] Kreith F, Manglik R M. *Principles of Heat Transfer*, 8th edn. Boston (USA): Cengage learning, 2016.

[51] Greenwood J A. An interpolation formula for flash temperatures. *Wear* **150**(1–2): 153–158 (1991)

[52] Tian X F, Kennedy Jr F E. Maximum and average flash temperatures in sliding contacts. *J Tribol* **116**(1): 167–174 (1994)

[53] Blok H. Theoretical study of temperature rise at surface of actual contact under oiliness lubricating conditions. *Proc Instn Mech Engrs* **2**: 222 (1937).

[54] Smith E H, Arnell R D. A new approach to the calculation of flash temperatures in dry, sliding contacts. *Tribol Lett* **52**(3): 407–414 (2013)

[55] Lee Y W, Liu Y W, Barber J R, Jang Y H. Thermal considerations during transient asperity contact. *Tribol Int* **94**: 87–91 (2016)

[56] Liu Y W, Barber J R. Transient heat conduction between rough sliding surfaces. *Tribol Lett* **55**(1): 23–33 (2014)

[57] Lee Y W, Liu Y W, Barber J R, Jang Y H. Thermal boundary conditions in sliding contact problem. *Tribol Int* **103**: 69–72 (2016)

[58] Jones D P, Leach D C, Moore D R. Mechanical properties of poly(ether-ether-ketone) for engineering applications. *Polymer* **26**(9): 1385–1393 (1985)

[59] Tanaka K, Kawakami S. Effect of various fillers on the friction and wear of polytetrafluoroethylene-based composites. *Wear* **79**(2): 221–234 (1982)

[60] Blanchet T A, Kennedy F E. Sliding wear mechanism of polytetrafluoroethylene (PTFE) and PTFE composites. *Wear* **153**(1): 229–243 (1992)

[61] Zhang G, Schlarb A K. Correlation of the tribological behaviors with the mechanical properties of poly-ether-ether-ketones (PEEKs) with different molecular weights and their fiber filled composites. *Wear* **266**(1–2): 337–344 (2009)

[62] Ghosh B, Xu F, Hou X H. Thermally conductive poly(ether ether ketone)/boron nitride composites with low coefficient of thermal expansion. *J Mater Sci* **56**(17): 10326–10337 (2021)

[63] Hsu K L, Kline D E, Tomlinson J N. Thermal conductivity of polytetrafluoroethylene. *J Appl Polym Sci* **9**(11): 3567–3574 (1965)

[64] Mu L W, Shi Y J, Feng X, Zhu J H, Lu X H. The effect of thermal conductivity and friction coefficient on the contact temperature of polyimide composites: Experimental and finite element simulation. *Tribol Int* **53**: 45–52 (2012)

[65] Calleja G, Jourdan A, Ameduri B, Habas J P. Where is the glass transition temperature of poly(tetrafluoroethylene)? A new approach by dynamic rheometry and mechanical tests. *Eur Polym J* **49**(8): 2214–2222 (2013)

[66] Liang C Y, Krimm S. Infrared spectra of high polymers. III. Polytetrafluoroethylene and polychlorotrifluoroethylene. *J Chem Phys* **25**(3): 563–571 (1956)

[67] Przedlacki M, Kajdas C. Tribochemistry of fluorinated fluids hydroxyl groups on steel and aluminum surfaces. *Tribol Trans* **49**(2): 202–214 (2006)

[68] Cole K C, Casella I G. Fourier transform infrared spectroscopic study of thermal degradation in films of poly(etheretherketone). *Thermochimica Acta* **211**: 209–228 (1992)

[69] Nguyen H X, Ishida H. Molecular analysis of the crystallization behavior of poly(aryl-ether-ether-ketone). *J Polym Sci B Polym Phys* **24**(5): 1079–1091 (1986)

[70] Doan V, Köppe R, Kasai P H. Dimerization of carboxylic acids and salts: An IR study in perfluoropolyether media. *J Am Chem Soc* **119**(41): 9810–9815 (1997)

[71] Harris K L, Pitenis A A, Sawyer W G, Krick B A, Blackman G S, Kasprzak D J, Junk C P. PTFE tribology and the role of mechanochemistry in the development of protective surface films. *Macromolecules* **48**(11): 3739–3745 (2015)

[72] Pitenis A A, Harris K L, Junk C P, Blackman G S, Sawyer W G, Krick B A. Ultralow wear PTFE and alumina composites: It is all about tribochemistry. *Tribol Lett* **57**(1): 4 (2015)

[73] Sun W, Liu X J, Liu K, Xu J M, Wang W, Ye J X. Paradoxical filler size effect on composite wear: Filler–matrix interaction and its tribochemical consequences. *Tribol Lett* **68**(4): 131 (2020)
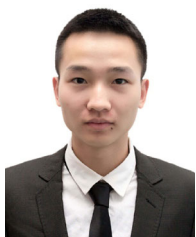
Zhibin LIN. He received his bachelor's degree in automotive engineering from Jilin University, China, in 2017. He is currently a Ph.D. candidate in the State Key Laboratory of Automotive Simulation and Control at Jilin University, China. His current research focuses on hybrid wear behaviors of polymer composite, tribofilm analysis, and tribology equipment development.

Guibin WANG. He received his Ph.D. degree in polymer chemistry and physics from Jilin University, China, in 2000. He joined the Special Engineering Plastics Engineering Research Center of the Ministry of Education, Jilin University, China, from 2002. His current position is a professor of the laboratory. His research areas cover the synthesis and molding of high-performance polymers, functionalization of resin matrix composites, and high-performance polymers.

Bingzhao GAO. He received his B.S. and M.S. degrees in vehicle engineering from Jilin University, China, in 1998 and 2002, respectively, and his Ph.D. degrees in mechanical engineering from Yokohama National University, Japan and in control engineering from Jilin University, China, in 2009. He is currently a professor with Tongji University, China. His current research interests include vehicle drivetrain design and intelligent vehicle.

Guowei FAN. He received his M.S. and Ph.D. degrees from Harbin Institute of Technology, China, in 2008 and 2012, respectively. Now he is an associate professor with the College of Instrumentation and Electrical Engineering, Jilin University, China. His research interest covers model predictive control, optimal and robust control, and applications in satellite attitude control.